Proceedings World Geothermal Congress 2000
Kyushu - Tohoku, Japan, May 28 - June 10, 2000

USING NUMERICAL SIMULATION OF ELECTROKINETIC POTENTIALS IN GEOTHERMAL RESERVOIR MANAGEMENT

Tsuneo Ishido[1] and John Pritchett[2]
[1] Geological Survey of Japan, 1-1-3 Higashi, Tsukuba 305-8567, Japan
[2] Maxwell Technologies Inc., 8888 Balboa Ave., San Diego, California 92123-1506, USA

Key Words: self-potential, reservoir monitoring, electrokinetic coupling, numerical simulation

ABSTRACT

Software has recently been developed to calculate space/time distributions of electrokinetic potentials resulting from histories of underground conditions (pressure, temperature, vapor saturation, concentration of dissolved species, flow rate, etc.) computed by unsteady multi-dimensional geothermal reservoir simulations (Ishido and Pritchett, 1999). The "EKP postprocessor" can be applied to "history-matching" of self-potential (SP) data since SP changes are caused principally by electrokinetic effects, particularly in the early stages of field exploitation. To assess the feasibility of using repeat SP surveys for reservoir monitoring, we carried out numerical simulations based on a mathematical model of a moderate-temperature two-phase reservoir. The results confirm the electrokinetic origin of production-induced changes in SP proposed by Ishido et al. (1989), and show that SP will respond to field-wide flow rate changes rapidly (within a month or so). This suggests that frequently-repeated SP surveys and/or continuous SP monitoring at times of flow rate changes will provide useful supplementary data for reservoir management.

1. INTRODUCTION

Numerical models of geothermal reservoirs are never precise, owing to the problem of non-uniqueness. The difficulty increases as the amount of available relevant field data becomes smaller. If only a few facts are known about the reservoir, a variety of theoretical reservoir models may explain these known facts equally well, but yield very different predictions of future potential. As the amount of field data available increases, of course, these uncertainties diminish. Thus, as time goes on, the understanding of the reservoir improves and forecasts become more reliable. Typically, the data base upon which numerical reservoir models are constructed consists of (1) geophysical surveys of various types, usually performed prior to development, (2) geological interpretations of underground structure, (3) downhole pressure and temperature surveys in shut-in wells, (4) flowing downhole surveys in wells, and (5) pressure-transient test results. Once exploitation begins in earnest, additional data become available such as temporal trends in downhole flowing pressures and wellhead enthalpies. These latter data may be used in "history-matching" studies.

Since the uncertainty in the predictions of numerical reservoir models is directly related to the amount of field data available against which the models can be tested, it is clear that the addition of repeat geophysical survey data to the above list of pertinent field measurements is likely to improve the reliability of these forecasts. It is well known in this connection that repeat precision gravity surveying has considerable promise for appraising the volumetric properties of any proposed mathematical reservoir model (see e.g. Ishido et al., 1995). The application of improved geophysical and geochemical techniques to reservoir management is one of the objectives of a geothermal R&D project (Horikoshi et al., 1998) entitled "Development of Technology for Reservoir Mass and Heat Flow Characterization", carried out by NEDO (the New Energy and Industrial Development Organization). This project is funded by MITI's New Sunshine Program; the Geological Survey of Japan carries out supporting basic research in cooperation with NEDO. We are pursuing the development of improved field survey techniques and associated modeling studies involving geophysical survey techniques and their application to reservoir performance monitoring, such as repeat self-potential, resistivity, and seismic velocity surveys, in addition to gravity monitoring.

Once the power station begins to operate, the natural underground flow pattern is likely to be immediately overwhelmed by perturbations caused by production and injection wells. This will bring about abrupt changes in the self-potential distribution through electrokinetic coupling. No other SP-source effects such as thermoelectric coupling and chemical diffusion potential will play significant roles, since production-induced changes in the distribution of temperature and fluid chemistry will be minor compared to flow pattern changes, especially in the early stages of field exploitation. In this paper, we first summarize salient features of the "EKP postprocessor" developed by Ishido and Pritchett (1999) and the electrokinetic mechanisms responsible for production-induced SP changes proposed by Ishido et al. (1989). Then we present numerical simulation studies to assess the feasibility of repeat self-potential (SP) surveys for geothermal reservoir management.

2. THE EKP-POSTPROCESSOR

The fundamental equation which is solved by the "EKP postprocessor" (Ishido and Pritchett, 1999) is:

$$\nabla\cdot\mathbf{I}_{cond} = -\nabla\cdot\mathbf{I}_{drag} \quad (1)$$

where $\mathbf{I}_{cond}$ is a conduction current density caused by electric conduction and $\mathbf{I}_{drag}$ is a drag (convection) current density caused by charges moved by fluid flow:

$$\mathbf{I}_{cond} = -L_{ee}\,\nabla\phi \quad (2)$$
$$\mathbf{I}_{drag} = -L_{ev}\,\nabla\xi \quad (3)$$

where L_{ee} and L_{ev} are the electrical conductivity of the bulk fluid/rock composite and the cross-coupling coefficient of electrokinetic effects respectively; $\nabla\phi$ and $\nabla\xi$ are the electric potential gradient and pore pressure gradient respectively. The coupling coefficient L_{ev} is proportional to the zeta potential (ζ), the potential across the electrical double layer. If ζ is negative, positive charge is carried by the fluid flow and vice versa.

The EKP postprocessor simulates electric potentials caused by subsurface fluid flow using a two-step process. First, it calculates the distribution of L_{ee}, L_{ev} and $\mathbf{I}_{drag}$ from the reservoir-simulation results using the same spatial grid used for the reservoir simulation calculation (called the RSV-grid hereafter). Next, the postprocessor calculates the electric potential (ϕ) distribution by solving Eqs. 1-3 within a finite-difference grid which is usually much greater in spatial extent than the RSV-grid (hereafter called the SP-grid), within which the RSV-grid is embedded.

Within the portion of the SP-grid overlapped by the RSV-grid, the distribution of electrical conductivity is obtained directly from RSV-grid values. Elsewhere within the SP-grid, the electrical conductivity distribution is user-specified and time-invariant. Ordinarily, boundary conditions on the potential are: zero normal gradient on the ground surface (upper surface) and zero potential along the bottom and vertical sides of the SP-grid. Eqs. 1-3 are solved numerically for the electrical potential distribution using a Gauss-Seidel iteration procedure which involves intermittent automatic optimization of the overrelaxation factor.

3. PRODUCTION-INDUCED SP CHANGE

Production-induced changes in reservoir pressure can bring about changes in self-potential (SP) in two ways. One is that they change the electrokinetic component of the natural SP distribution by modifying the natural convective flow pattern (see Fig. 1). A change in the SP distribution between 1981 and 1984 observed at the Nigorikawa caldera, where the Mori geothermal power plant has been in continuous operation since 1982, is thought to be this type (Ishido and Pritchett, 1999).

The other mechanism, proposed by Ishido et al. (1989), is that an underground fluid sink or source (production or injection well) will generate an SP anomaly at the ground surface if the pressure change propagates to a boundary separating regions of differing streaming potential coefficient (C) where $C= -L_{ev}/L_{ee}, < 0$ for ordinary geologic situations). For the cases shown in Figs. 2(a) and (b), the magnitude of the streaming potential coefficient in region 2 (the caprock) is smaller than that in region 1 (the reservoir), so $C_1 < C_2 < 0$. Generally speaking, the reduction in the magnitude of C is brought about by either a lower L_{ev} magnitude (due to lower temperature or higher salinity) or by higher L_{ee} (due to higher salinity, significant contribution of the surface conductivity or the presence of conductive minerals such as shales and clays). Therefore, the caprock overlying a geothermal reservoir will typically have a lower-magnitude C value than that of the reservoir itself. The polarity of the SP anomaly can be predicted by the total potential approach (Fitterman, 1987). The total potential (ψ) is defined as $\psi = \phi + C\,\Delta P$, where ϕ and ΔP are the electric potential and fluid pressure change, respectively. Production-induced pressure change along the C boundary brings about sources (current dipoles) of total potential. If the pressure change is negative (positive), the current dipole for Ψ points to the side of larger (smaller) C. As shown in Figs. 2(a) and (b), positive and negative SP anomalies will form over the production and injection zones, respectively.

If substantial production-induced expansion of the vapor dominated zone takes place due to reservoir pressure decline, a C-boundary will be created near the bottom of the two-phase zone (Fig. 3). Since the conductivity of the two-phase zone is less than that of the underlying all-liquid zone, the two-phase region will be characterized by a larger magnitude of C (so long as the liquid phase will flow). Thus, $C_2 < C_1 < 0$. So, in this case, production-induced pressure decrease brings about negative SP on the ground surface. SP changes observed at the Okuaizu geothermal field are thought to be this type (Tosha et al., 2000). SP changes at the Sumikawa geothermal field have more complex features (Matsushima et al., 2000), probably explained by a combination of the type shown in Fig. 2 and that shown in Fig. 3.

4. NUMERICAL SIMULATION OF EK POTENTIALS

The hypothetical reservoir model used for the present feasibility study is basically the same as the conceptual model developed by Yano and Ishido (1995) for numerical studies of the natural evolution of the two-phase reservoir which formed along the Ginyu fault in the Ogiri field, Kyushu island, Japan (Fig. 4). The two-dimensional model is oriented east-west and incorporates the major structural features of the Ginyu reservoir. The high-permeability reservoir *(A* in Fig. 4) is overlain by the low-permeability altered caprock *(C)*. The model incorporates a 50-m-wide permeable vertical flow path (corresponding to a fractured zone, *F)* between the reservoir and the ground surface. This vertical fracture zone serves to supply the Ginyu fumarole area with steam. At depth, 36 kg/s of hot (260°C) water is assumed to recharge the reservoir through a permeable conduit *(E)*. A permeable horizontal conduit *(H)* allows for lateral mass outflow. The *S* and *B* rocks surrounding the reservoir are more permeable than the caprock, but the permeability of rock *B* is low enough that conduction is the dominant mode of heat transfer. The hot recharge water boils as it rises through the system. In the upper part of the reservoir, part of this fluid becomes pure steam, which then flows to the surface through the fracture in the caprock and fuels the Ginyu fumaroles. The rest of the hot water leaves the reservoir to the west through horizontal conduit *H*. Substantial fluid flows also take place in the shallow *S* formation above the caprock due to topography effects.

Porosities and permeabilities of the formations shown in Fig. 4 are listed in Table 1. The two-dimensional RSV-grid is 250 m thick. All exterior boundaries except the top surface and a part of the western vertical surface are impermeable and insulated; pressure and temperature are maintained at 1 bar and 20°C respectively along the top boundary, and the sea-level pressure on the western boundary is maintained at 40 bars. Any “fresh water” which flows downward into the grid through the top surface contains a dilute tracer to permit its identification. A source of high-temperature “magmatic water” (similarly tagged with a dilute tracer) is imposed at the bottom of the deep conduit. The development of the hydrothermal convection system was then computed using the STAR geothermal simulator (Pritchett, 1995). The system reached quasi-steady state after around 5000 years of evolution. The STAR

simulator was next used to perform a 30-year forecast of the consequences of production and injection, starting from the natural-state model described above as the initial conditions. All boundary conditions and rock properties were the same as used to calculate the natural-state. Three hypothetical production wells and two injection wells were incorporated in the model. A constant total power station steam flow rate of 45 kg/s (sufficient to generate 20 MW_e of electricity) was assumed. A fixed separator pressure of 2.5 bars was used, and all separated liquid water and a small amount of steam condensate were reinjected.

The EKP postprocessor (Ishido and Pritchett, 1999) for the STAR code was applied to forecast SP changes induced by the above fluid production/reinjection operations. For the self-potential calculations, the magmatic fluid is assumed to contain NaCl; the concentrations are proportional to the mass fraction of magmatic dilute tracer, and NaCl is 0.02 mol/l in the pure upflowing magmatic fluid entering from below. The fresh water is assumed to contain dilute NaCl (0.002 mol/l). For the calculations of L_{ev}, ΔpH is taken equal to 5 for all rock formations listed in Table 1 except the caprock (for which ΔpH = 0 to make $\zeta = L_{ev} = C = 0$); see Ishido and Pritchett (1999) for an explanation of ΔpH. It is assumed that $\mathbf{I}_{drag}$ is not reduced for two-phase flow (containing a vapor phase which cannot move charge) so long as the liquid phase flows. The postprocessor calculates L_{ee}, L_{ev} and $\nabla \cdot \mathbf{I}_{drag}$ from the distributions of composition and other results from the STAR simulation (such as temperature, pressure, liquid saturation and fluid mass flux) within the RSV-grid. Then the distribution of electrical potential is calculated within the SP-grid. The SP-grid extends over -2850 m < x < +2850 m, -2850 m < y < +2850 m in the horizontal direction, and -3550 m < z < 850 m in the vertical direction. The two-dimensional RSV-grid occupies the region -2600 m < x < +1750 m, -125 m < y < +125 m, and -1550 m < z < 850 m. Within this portion of the SP-grid, the distribution of electrical conductivity is obtained directly from RSV-grid values. Elsewhere within the SP-grid, the electrical conductivity is assumed to be 0.002 S/m in the uppermost layer, 0.1 S/m at depths corresponding to the caprock region in the RSV-grid, and 0.02 S/m in the remaining lower layer.

Under natural-state conditions, the model predicts a large negative anomaly appears in a region, about 700 m west of the fumarole area, where meteoric water flows downward (Fig. 5(a)). The descending meteoric water removes positive charge from the neighborhood of the ground surface and thus produces a conduction current sink (see Fig. 6). Although the fumarole area is high in elevation, no significant downward flow takes place due to the presence of both the vapor upflow and the impermeable caprock, so SP is relatively high compared to the surrounding area. These results from the present simple model reproduce the SP distribution observed in and around the Ginyu fumarole area quite well (Ishido et al., 1990). The large positive anomaly about two kilometers west of the fumarole area corresponds to the region where upflowing meteoric water emerges from the ground surface.

The SP distributions during exploitation were calculated using the same parameter set as that used in the natural-state model. The model shows that although the flow pattern is dominated by production-induced flow, the SP distribution pattern is similar to the natural-state (compare Fig. 5(b) to 5(a)). As shown in Fig. 7(a), SP around the fumarole area decreases slightly during the first three months of field operation, then begins to increase and becomes stable after about two years. In the production area, substantial production-induced expansion of the vapor-dominated zone takes place during the early stages of field operation. Just below the vapor zone, vigorous boiling takes place and counterflows of vapor (upward) and liquid (downward) are produced. This downward flow of the liquid phase carries electric current ($\mathbf{I}_{drag}$) with it and brings about a negative SP change on the ground surface. This negative change ceases in a relatively short time (about six months) in the present case. The electrical conductivity of the reservoir formation decreased from ~0.1 S/m to less than 0.01 S/m as the pore fluid changed from liquid to vapor.

As seen in Fig. 6, sources and sinks of conduction current appear to correspond spatially to the feedpoints of production and reinjection wells respectively. If the production-induced pressure change is localized at depth, the electrical potential change is limited to the region of pressure change if C (the streaming potential coefficient) is homogeneous (Ishido, 1989). However, in the present case, although the region of pressure increase is generally confined below the caprock, this region encounters the overlying zero-C caprock from below, so conduction current can be produced at the ground surface. In the production area, the effects of the current sources become dominant after about one year of field operation (Fig. 7(a)). In the reinjection area, the current sinks are relatively shallow, so the SP decrease is relatively large; about 30 mV after three months of field operation. This negative change overlaps the western part of natural negative anomaly (Fig. 5(b)) and is quite stable (Fig. 7(b)). As seen in Fig. 7, the response to one- month shut-in of all production/reinjection wells after a year of field operation is striking in the reinjection area, but is more subtle (and probably imperceptible in practice) in the production area.

Electrically-conductive well casings are thought to distort the potential around them. Therefore, for comparison, we re-calculated the SP distributions incorporating additional vertical conductivity in the grid blocks penetrated by the wells. Modeling predicts the difference between results with and without the "conductive well casings" is negligible under natural-state conditions. However, under exploitation conditions, the effects of "conductive well casings" are substantial. The effects of current sources within the production area appear at the ground surface because of the additional vertical conductivity, and the current sinks within the reinjection area produce negative anomalies localized around the well field (compare Fig. 5(c) to 5(b)). The response to the one-month shut-in becomes large enough to be easily detected in the production area if "conductive well casings" are included (compare Fig. 8 to 7).

5. CONCLUDING REMARKS

Fig. 9 shows the calculated distribution of ground-surface microgravity change at 2.5 years based upon the present exploitation model used for the SP calculations. Gravity declines substantially above the production area because of steam volume increase within the two-phase zone below the caprock. In contrast, a slight positive anomaly near the reinjection area is probably too small to be detected. It is noteworthy that gravity appears to be more sensitive to the production region, whereas SP is more responsive to the injection zone. The same conclusion was drawn from an application of the present EKP postprocessor to a different hypothetical reservoir model (Pritchett et al., 2000).

In situations where the negative anomalies associated with the expansion of a two-phase zone dominate, significant SP changes will be expected in production areas as well. At the Okuaizu field, this type of anomaly was found to change significantly during a two-month shut-in of all production wells (Tosha et al., 2000). Since SP is sensitive to flow pattern changes, substantial changes in SP can be seen at times of field-wide flow rate change even if the observation period is as short as one month. Frequently-repeated SP surveys and/or continuous SP monitoring in and around the production and reinjection areas can therefore provide useful data for improving mathematical reservoir models by history-matching.

ACKNOWLEDGEMENTS

The present study was funded by MITI's New Sunshine Program. The STAR/EKP simulations were run on the IBM Cluster System at the MITI-TACC computing complex in Tsukuba.

REFERENCES

Fitterman, D.V. (1978). Electrokinetic and magnetic anomalies associated with dilatant regions in a layered earth. *J. Geophys. Res.*, Vol. 83, pp.5923-5928.

Horikoshi, T., Nagahama, N., and Okubo, Y. (1998). Reservoir mass and heat flow characterization. *Geothem. Resour. Counc. Trans.*, Vol. 22, pp.165-169.

Ishido, T. (1989). Self-potential generation by subsurface water flow through electrokinetic coupling. In: *Detection of Subsurface Flow Phenomena,* Lecture Notes in Earth Sciences, Vol. 27, G.-P. Merkler et al. (Eds), Springer-Verlag, Berlin, pp.121-131.

Ishido, T., Kikuchi, T., and Sugihara, M. (1989). Mapping thermally driven upflows by the self-potential method. In: *Hydrogeological Regimes and Their Subsurface Thermal Effects*, Geophys. Monogr., 47, IUGG Vol. 2, A.E. Beck et al. (Eds), AGU, pp.151-158.

Ishido, T., Kikuchi, T., Yano, Y., Sugihara, M., and Nakao, S. (1990). Hydrogeology inferred from the self-potential distribution, Kirishima geothermal field, Japan. *Geothem. Resour. Counc. Trans.*, Vol.14-part II, pp.916-926.

Ishido, T. and Pritchett, J.W. (1999). Numerical simulation of electrokinetic potentials associated with subsurface fluid flow. *J. Geophys. Res.*, Vol. 104, pp. 15,247-15,259.

Ishido, T., Sugihara, M., Pritchett, J.W., and Ariki, K. (1995). Feasibility study of reservoir monitoring using repeat precision gravity measurements at the Sumikawa geothermal field. In: *Proc. World Geothermal Congress '95*, Florence, pp.853-859.

Matsushima, N., Kikuchi, T., Tosha, T., Nakao, S., Yano, Y., Ishido, T., Hatakeyama, K., and Ariki, K. (2000). Repeat SP measurements at the Sumikawa geothermal field, Japan. In: *Proc. World Geothermal Congress 2000*, Japan (in press).

Pritchett, J.W. (1995). STAR: a geothermal reservoir simulation system, In: *Proc. World Geothermal Congress '95*, Florence, pp.2959-2963.

Pritchett, J., Stevens, J., Wannamaker, P., Nakanishi, S., and Yamazawa, S. (2000). Theoretical feasibility studies of reservoir monitoring using geophysical survey techniques. In: *Proc. World Geothermal Congress 2000*, Japan (in press).

Tosha, T., Ishido, T., Matsushima, N., and Nishi, Y. (2000). Self-potential variation at the Yanaizu-Nishiyama geothermal field and its interpretation by the numerical simulation. In: *Proc. World Geothermal Congress 2000*, Japan (in press).

Yano, Y. and Ishido, T. (1995). Numerical modeling of the evolution of two-phase zones under a fractured caprock. *Geothermics*, Vol. 24, pp.507-521.

Table 1 Rock properties used in the numerical simulation

Formation	Porosity	Permeability (mdarcy)
A (reservoir)	0.1	100
B	0.01	3
C (caprock)	0.01	0.01
E	0.05	100
F	0.05	5
H	0.1	100
S	0.1	10

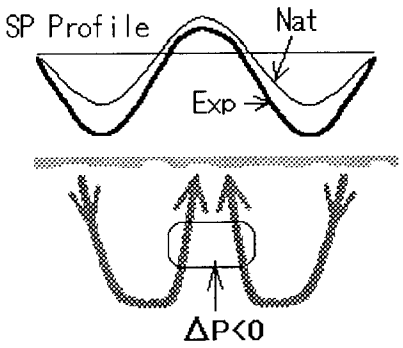

Fig. 1 An electrokinetic model for production-induced SP change. Natural-state SP can be changed by pressure decline due to production which modifies the natural convective flow.

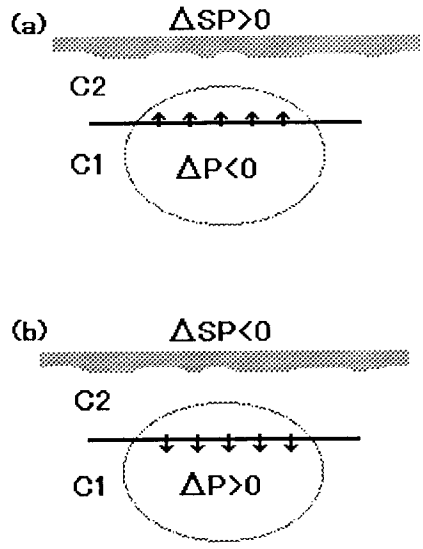

Fig. 2 Electrokinetic models for SP changes in (a) production and (b) injection areas. C1 and C2 denote the streaming potential coefficients for the reservoir and caprock regions respectively. The arrows show the current dipoles which act as sources of the total potential.

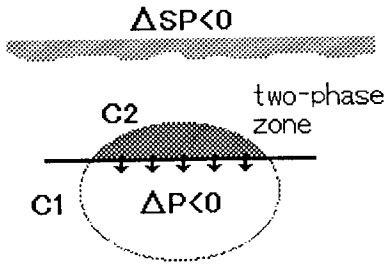

Fig. 3 An electrokinetic model for production-induced SP change. The streaming potential coefficient in the two-phase zone (C2) is larger in magnitude than the original C1 for the reservoir.

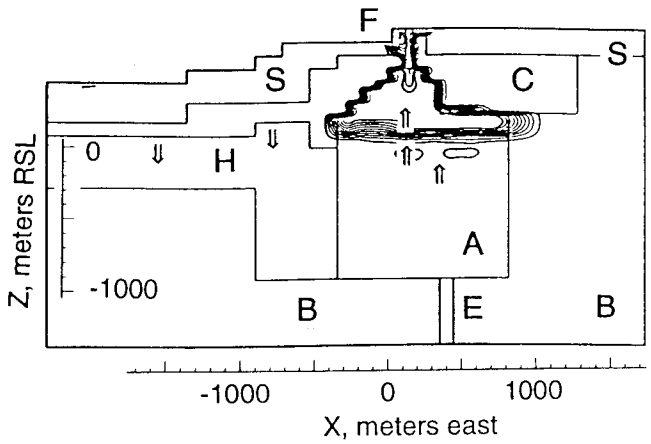

Fig. 4 Distribution of rock formations used in the numerical simulation. Also shown are locations of feedpoints of production and reinjection wells (arrows) and distribution of vapor saturation after 20 years of fluid production and reinjection (contours). The properties of rock units A, B, C, E, F, H and S are shown in Table 1.

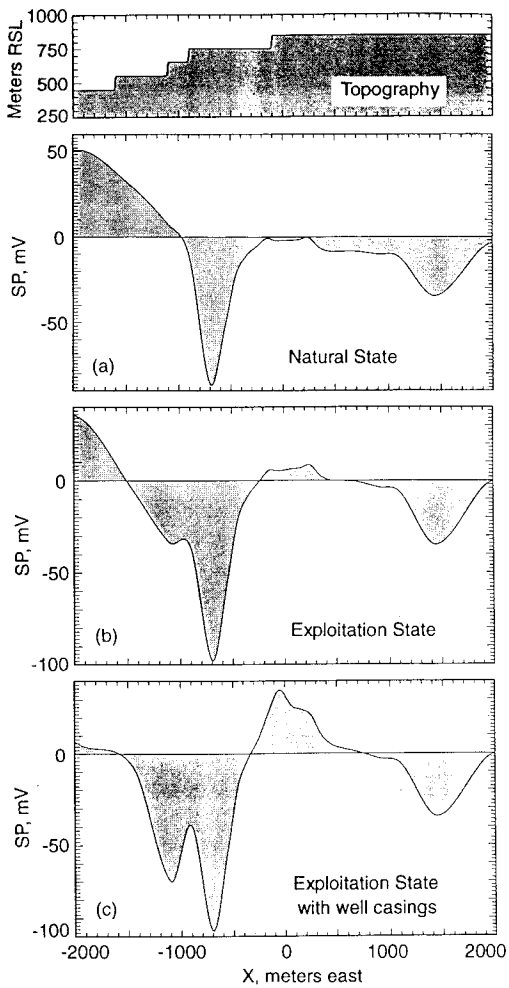

Fig. 5 Calculated ground-surface self-potential distribution (a) for natural-state, and after one year of fluid production and reinjection for cases (b) without and (c) with additional conductivity brought about by iron well casings.

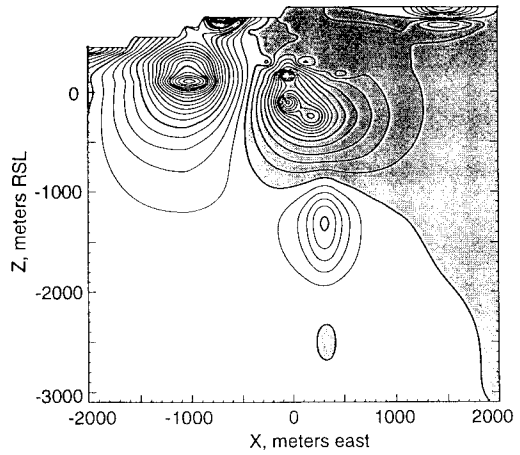

Fig. 6 Vertical contour plot of calculated electric potential after one year of fluid production and reinjection. Corresponding surface profile is shown in Fig. 5(b). Contour interval is 5 mV. SP is positive in the shaded area.

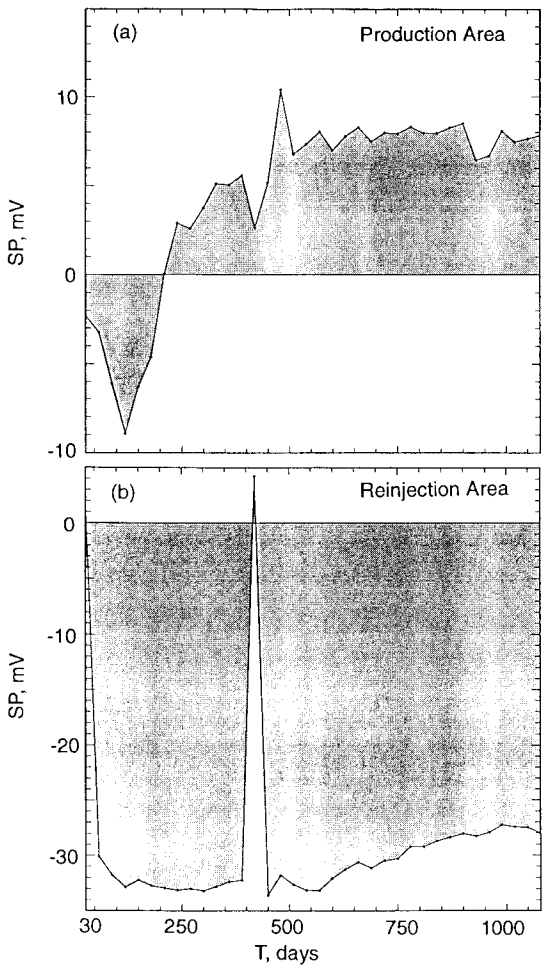

Fig. 7 Changes in SP with time at (a) production area (x = 0 m) and (b) reinjection area (x = -1000 m). Production and reinjection start at t = 30 days and stop for 30 days between t = 390 days and t = 420 days.

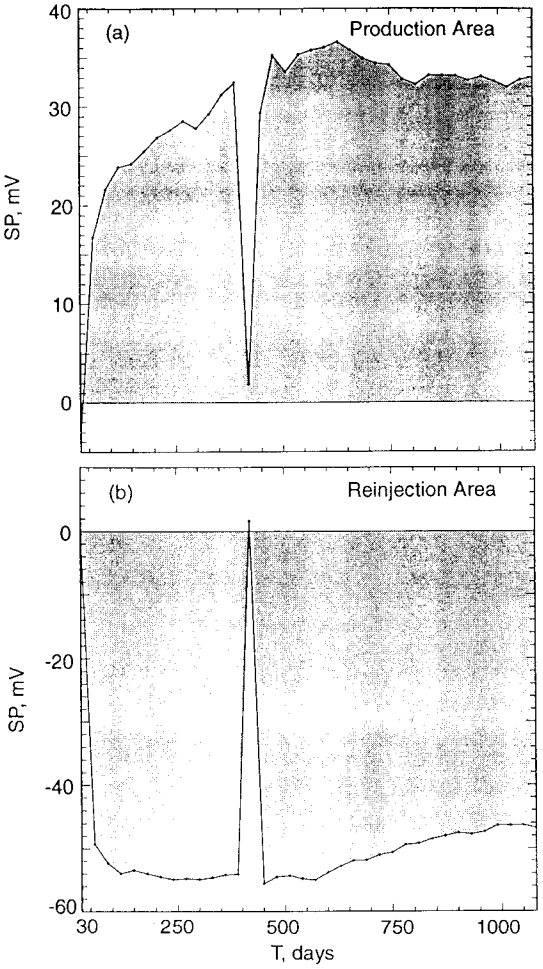

Fig. 8 Changes in SP with time for case with additional conductivity brought about by iron well casings at (a) production area (x = 0 m) and (b) reinjection area (x = -1000 m). Production and reinjection start at t = 30 days and stop for 30 days from t = 390 days to t = 420 days.

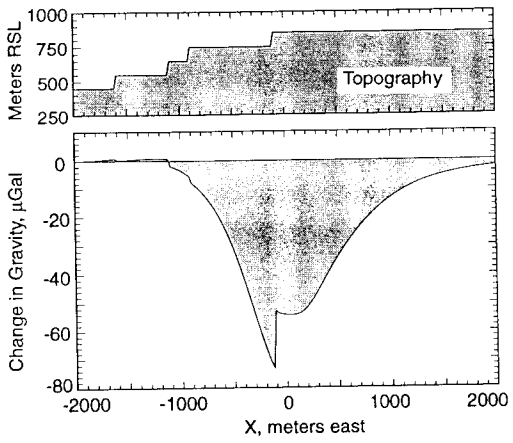

Fig. 9 Calculated microgravity change after 2.5 years of fluid production and reinjection.